Environ Earth Sci (2013) 70:33–47
DOI 10.1007/s12665-012-2101-5

ORIGINAL ARTICLE

Catchment-scale soil erosion and sediment yield simulation using a spatially distributed erosion model

Giha Lee · Wansik Yu · Kwansue Jung · APIP

Received: 29 August 2011 / Accepted: 29 October 2012 / Published online: 15 November 2012

Abstract Increasing rainfall intensity and frequency due to extreme climate change and haphazard land development are aggravating soil erosion problems in Korea. A quantitative estimate of the amount of sediment from the catchment is essential for soil and water conservation planning and management. Essential to catchment-scale soil erosion modeling is the ability to represent the fluvial transport system associated with the processes of detachment, transport, and deposition of soil particles due to rainfall and surface flow. This study applied a spatially distributed hydrologic model of rainfall–runoff–sediment yield simulation for flood events due to typhoons and then assessed the impact of topographic and climatic factors on erosion and deposition at a catchment scale. Measured versus predicted values of runoff and sediment discharge were acceptable in terms of applied model performance measures despite underestimation of simulated sediment loads near peak concentrations. Erosion occurred widely throughout the catchment, whereas deposition appeared near the channel network grid cells with a short hillslope flow path distance and gentle slope; the critical values of both topographic factors, providing only deposition, were observed at 3.5 (km) (hillslope flow path distance) and 0.2 (m/m) (local slope), respectively. In addition, spatially heterogeneous rainfall intensity, dependent on Thiessen polygons, led to spatially distinct net-erosion patterns; erosion increased gradually as rainfall amount increased, whereas deposition responded irregularly to variations in rainfall.

Keywords Topographic and climatic factors · Catchment-scale soil erosion modeling · Erosion and deposition · Rainfall–runoff–sediment yield

G. Lee (✉)
Land, Transport and Maritime Affairs Team,
National Assembly Research Service, Seoul 150-703, Korea
e-mail: leegiha@gmail.com

W. Yu
Department of Civil and Earth Resources Engineering,
Kyoto University, Kyoto 611-0011, Japan
e-mail: yuwansik@gmail.com

K. Jung
Department of Civil Engineering, Chungnam National
University, Daejeon 305-764, Korea
e-mail: ksjung@cnu.ac.kr

APIP
Disaster Prevention Research Institute, Kyoto University,
Uji, Kyoto 611-0011, Japan
e-mail: apipkazumi@gmail.com

Introduction

Accelerated soil erosion and sediment yield due to extreme climate change, such as increased rainfall intensity, and human-induced environmental changes such as haphazard land development, are widely recognized problems around the world. In particular, Korea has mountainous regions representing more than 70 % of the country, and land cover is very shallow and mostly composed of weathered gneiss, making Korea vulnerable to soil loss and landsides (Lee et al. 2007, 2008). The National Resources Conservation Service (NRCS) classified Korea as a nation with very high water erosion vulnerability (http://www.soils.usda.gov/use/worldsoils/mapindex/erosh2o.html).

Erosion or sediment disasters repeat annually due to localized heavy rain and frequent typhoons during a rainy season from June to September and consequently result in incalculable damage to many areas of the country (Chae

et al. 2010). In addition, the restoration cost for this damage is measured in millions of dollars, each year (Park and Son 1998). Therefore, continuous scientific efforts are made to improve understanding of erosion and sediment transport processes at field, catchment, and larger regional scales from the quantitative perspective to assess their on- and off-site impacts on land resource management and to mitigate erosion- or sediment-induced damage (Morris and Fan 1997).

However, it is difficult and costly to observe and measure erosion processes continuously during runoff or erosion events because of the spatial and time scales at which the processes occur. Therefore, erosion models are used to predict erosion and sediment (Jetten et al. 2003). Erosion modeling is based on an understanding of physical laws and landscape processes (such as runoff and soil formation) occurring in the natural environment. The key to erosion modeling is the ability to represent the fluvial transport system associated with detachment, transport, and deposition of soil particles due to rainfall and surface flow along flow pathways of a catchment (Storm et al. 1990; Toy et al. 2002; Kalin and Hantush 2003).

Over the last 20 years, there has been remarkable progress in the development of mathematical tools for erosion and sediment transport modeling, with a tendency toward process-based model development (Nearing et al. 1989; Vente and Poesen 2005). EUROSEM (Morgan et al. 1992, 1998), WEPP (Flanagan and Nearing 1995), and KINEROS (Woolhiser et al. 1990) are well-known tools; in these models, the topography was represented by a cascade of plane and channel elements in a spatially distributed manner. In other words, these models can make predictions that are distributed in space, with state variables that represent local averages of storage, flow depths, or hydraulic potential, by discretizing the catchment into a large number of irregular polygons or grid squares and solving the equations for the state variables associated with every element. These models currently integrate with geographic information systems (GIS) to take account of spatial heterogeneity in various hydrologic and geomorphologic variables (De Roo et al. 1996a, b). Thus, they predict where, when, and how much erosion or deposition is occurring (Johnson et al. 2000).

Environmental conditions determine types and rates of erosion and deposition occurring in a specific area. These conditions generally consist of following primary components or factors: climate, topography, soil, and land cover/use (Toy et al. 2002). As stated above, the physically based distributed erosion models are able to provide spatial information of catchment responses (e.g., surface runoff depth, erosion rate, deposition rate, and so on) to these factors; thus, they allow users to clarify a dominant factor of individual stages in erosion-sediment yield processes of a catchment. Rainfall is the single most important climatic variable affecting water erosion, as it is significantly related to soil detachment by raindrop and surface flow (Foster 1982). In addition, the important topographic variables are slope length and steepness (McCool et al. 1987, 1989). Erosion at a given location on a slope is a function of the distance from the surface runoff origin and the steepness at that location (Foster and Meyer 1977). If the location is far down the slope where much runoff has accumulated, the erosion rate will be high. For a given location, erosion will be proportional to the steepness at that location.

The goal of this study was to simulate soil erosion and sediment yield at a catchment scale using a physically based distributed erosion model and then demonstrate erosion and deposition patterns in time and space during heavy rainfall periods. Furthermore, we assessed the impact of topographic and climatic factors on erosion and deposition within a study area. For these objectives, we applied the model to the Cheoncheon catchment, upstream of Yongdam dam in Korea (Fig. 3) for three flood events caused by large typhoons. Measured versus predicted values of runoff and sediment discharge, and soil redistribution (due to erosion and deposition) were plotted and discussed. In addition, hillslope flow path distance and slope steepness were selected among diverse topographic factors, and the impact of such factors on spatial variation of erosion and deposition was analyzed and discussed. Finally, the GIS technique was used to analyze the relationship between spatially distributed rainfall and erosion or deposition at each grid cell within the study site.

"Spatially distributed erosion model" introduces the concepts underlying the physically based distributed erosion model used in this study, and "Model application" describes the comparative results of streamflow and sediment discharge between simulation and observation in addition to erosion and deposition mapping. "Analysis of factors influencing soil erosion and deposition" addresses the relationships between topographic or climatic factors and erosion or deposition. Finally, "concluding remarks" summarizes major conclusions in this study.

Spatially distributed erosion model

In this study, we used an effective and robust spatially distributed erosion model consisting of two basic element modules: a rainfall–runoff module, based on the kinematic wave method for subsurface and surface flow with a conceptual stage-discharge relationship (Tachikawa et al. 2004), and an erosion-sediment yield module, based on the unit stream power method (Yang 1972) to model transport capacity of surface flow (Govers 1990; APIP 2008). More details of the model are introduced as follows.

Rainfall–runoff module

For soil erosion simulation, a rainfall–runoff module must accurately represent the distribution of rainfall, infiltration of the rainfall into the ground, and the routing of excess rainfall surface into the channel components and ultimately to the catchment outlet (Julien et al. 1995). In this study, we used the cell-based one-dimensional kinematic wave method for subsurface and surface flow simulation (hereafter, KWMSS), which was introduced by Takasao and Shiiba (1988) and enhanced by Tachikawa et al. (2004).

In this module, the drainage network is represented by sets of hillslope and channel elements from the digital elevation model (DEM) (Shiiba et al. 1999). Each element is represented by a rectangle formed by two adjacent nodes of grid cells, determined by the steepest gradient based on the eight flow directions (O'Callaghan and Mark 1984). Figure 1a is a schematic topographic representation of KWMSS; the arrows indicate element models for calculating hydrological variables, such as water flux. The rainfall over all hillslope elements, derived as above, flows one-dimensionally into the river nodes and then routes to the catchment outlet. The rainfall–runoff transformation conducted by KWMSS is based on the assumption that each hillslope element is covered with a permeable soil layer, as shown in Fig. 1b. This soil layer consists of a capillary layer and a non-capillary layer. In these conceptual soil layers, slow and quick flow are simulated as unsaturated Darcy flow and saturated Darcy flow, respectively, and surface flow occurs if water depth, h (m) exceeds soil water capacity. The KWMSS represents these runoff processes in the following manner (Tachikawa et al. 2004):

$$q = \begin{cases} v_c d_c (h/d_c)^{\beta}, & 0 \le h \le d_c \\ v_c d_c + v_a (h - d_c), & d_c \le h \le d_s \\ v_c d_c + v_a (h - d_c) + \alpha (h - d_s)^m, & d_s \le h \end{cases} \quad (1)$$

$$\frac{\partial h}{\partial t} + \frac{\partial q}{\partial x} = r(x,t) \quad (2)$$

The flow rate of each hillslope element q (m^2/s) is calculated by Eq. (1), combined with the continuity equation, Eq. (2), where $v_c = k_c i$ (m/s), $v_a = k_a i$ (m/s), $k_c = k_a/\beta$ (m/s), $\alpha = \sqrt{i}/n$ ($m^{1/3}s^{-1}$), $m = 5/3$, i is the slope gradient, k_c (m/s) is the hydraulic conductivity of the capillary soil layer, k_a (m/s) is the hydraulic conductivity of the non-capillary soil layer, n ($m^{-1/3}s$) is the roughness coefficient, d_s (m) is the water depth corresponding to the water content, and d_c (m) is the water depth corresponding to maximum water content in the capillary pore. Singh (2001) stated that the kinematic wave method was computationally efficient and suitable for simulating not only surface and channel routing but also subsurface flow at hillslopes. Furthermore, for a given rainfall event, rainfall is directly added to subsurface or surface flow on grid cells according to the water depth of each cell corresponding to parts of the rainfall input field. The KWMSS does not consider vertical flow due to infiltration, but represents lagged subsurface flow with calibrated hydraulic conductivities and soil layer thicknesses (Tachikawa et al. 2004).

Erosion-sediment yield module

The erosion-sediment yield module based on the unit stream power concept was linked with the KWMSS module systemically to compute soil detachment, transport, and deposition processes.

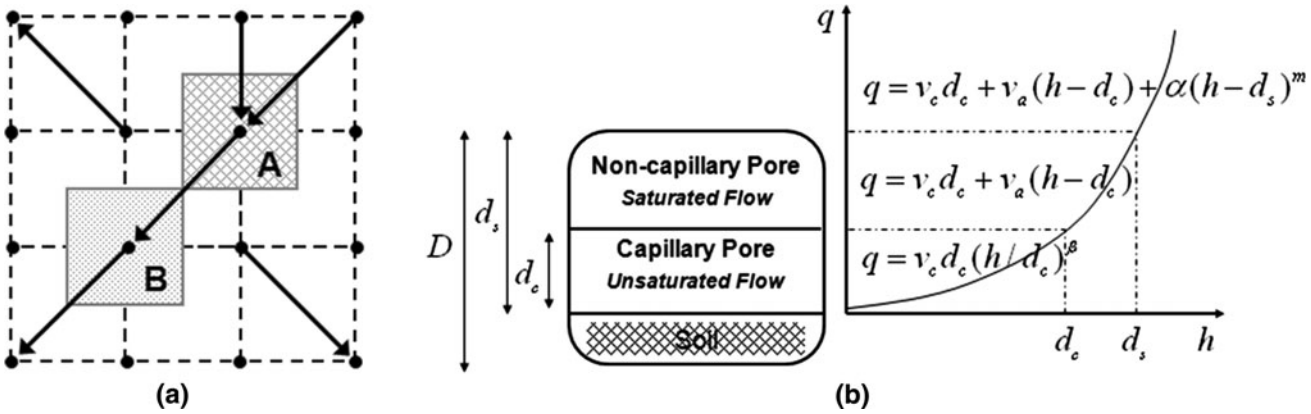

Fig. 1 **a** Schematic diagram of the KWMSS slope elements for delineating the drainage network; *each point indicates* grid center; the total area of element AB = ½ of grid area A + ½ of grid area B; **b** stage–discharge relationship of the KWMSS (Lee et al. 2009; reproduced with permission from ASCE)

Soil detachment and transport at each grid cell are simulated by Eqs. (3) and (4) with the raindrop detachment (DR) and surface flow detachment (DF).

$$\frac{\partial(h_s C)}{\partial t} + \frac{\partial(q_s C)}{\partial x} = e(x, t) \tag{3}$$

$$e(x, t) = \mathrm{DR} + \mathrm{DF} \tag{4}$$

where C (kg/m^3) is the surface flow sediment concentration, h_s (m) is the surface flow depth, q_s (m^2/s) is the discharge of surface flow, and e (kg/m^2/s) is the net-erosion. DR is calculated with an empirical equation, based on the assumption that the detachment rate is proportional to the kinetic energy of rainfall but decreases as surface flow depth increases, while DF is simulated as a function of surface flow and transport capacity (TC). Both DR and DF are calculated by Eqs. (5) and (6) at individual grid cells (Morgan et al. 1998).

$$\mathrm{DR} = k\mathrm{KE}e^{-bh_s} \tag{5}$$

$$\mathrm{DF} = \alpha\left(\frac{\mathrm{TC}}{1000} - C\right)h_s \tag{6}$$

where k(kg/J) is the soil detachability, KE (J/m^2) is the total kinetic energy of the net rainfall, b is the exponent to be tuned, and α is the non-dimensional detachment/deposition efficiency factor. The transport capacity determines the sediment transport rate due to surface flow on the ground surface and is generally defined as the maximum value of sediment concentration. Many (mostly empirical) equations have been developed to predict sediment flow transport capacity as a function of flow characteristics, slope, and material characteristics, and such equations often use a threshold value of stream power, shear stress, or discharge. Here, the transport capacity of surface flow is modeled as a function of the unit stream power and depends on the value of the median grain size (Yang 1972, 1973; Govers 1990). An equation for estimating TC is expressed as follows:

$$\mathrm{TC} = 10^{\log C_t} = 5.435 - 0.286\log\frac{\omega d}{\upsilon} - 0.457\log\frac{U_*}{\omega} + \left(1.799 - 0.409\log\frac{\omega d}{\upsilon} - 0.314\log\frac{U_*}{\omega}\right)\log\left(\frac{v_s i - v_{cr} i}{\omega}\right) \tag{7}$$

where C_t (mg/l) is the total sediment concentration, $v_s i$ (m/s) is the unit stream power (v_s is the surface flow velocity and i is the slope), $v_{cr} i$ (m/s) is the critical unit stream power (v_{cr} is the critical flow velocity), ω (m/s) is the sediment fall velocity, υ (m/s^2) is the kinematic viscosity of the water, and ($U_* = \sqrt{gih_s}$) (m/s) is the average shear velocity.

The algorithm of the erosion-sediment yield module is dependent on the comparison between transport capacity (TC) and sediment supply (Q_{sed}); when surface runoff occurs in a grid cell and the TC of flow is larger than the Q_{sed} from the upper grid cell, the sediment of TC $- Q_{sed}$ will be yielded (i.e., erosion). In contrast, if TC is smaller than $Q_{sed}$from the upper grid cell, the sediment of Q_{sed} − TC will be accumulated in a grid cell (i.e., deposition), as illustrated in Fig. 2 (Lane et al. 1988; Sayama 2003; APIP 2008).

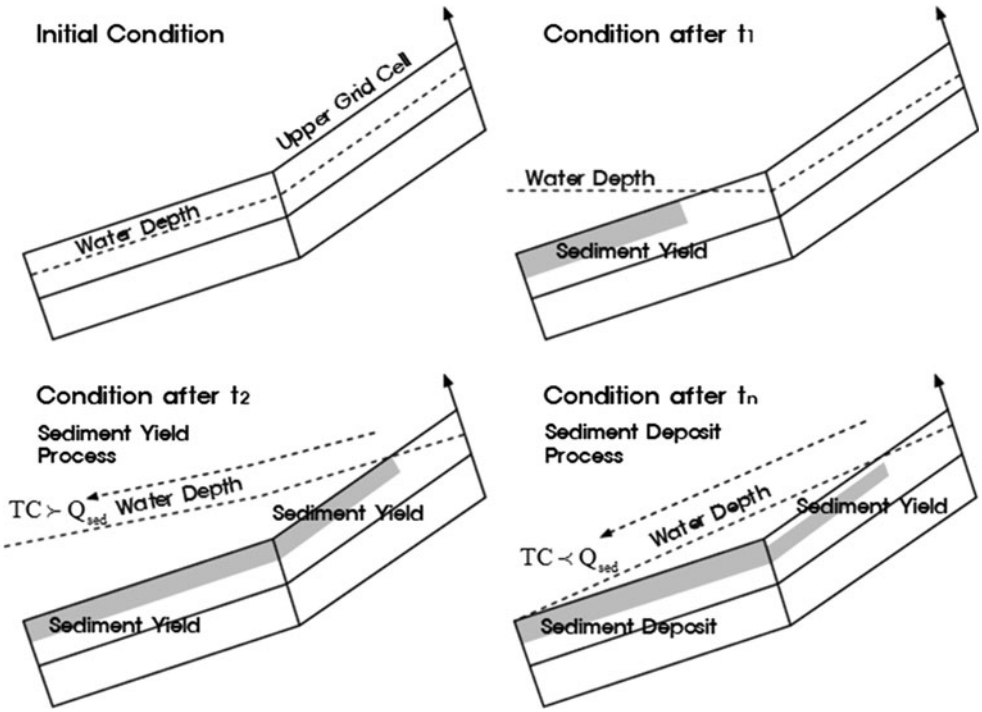

Fig. 2 Schematic illustration of sediment transport processes by flow on a slope (Sayama 2003; reproduced with personal permission)

The model with the two modules provides both catchment-aggregated responses, such as hydrographs and sedigraphs, and the spatial pattern of erosion and deposition within a modeling domain.

Model application

Study area and data

As illustrated in Fig. 3a, the Cheoncheon catchment (289.9 km^2) comprises about 31 % of the Yongdam dam basin (928.4 km^2) and is located in the west-central part of South Korea. The average elevation of the study site is 549.13 m and the slope is steep; this catchment is a mountainous area with high potential for sediment loss. Four rain gauges are within and near the Cheoncheon catchment (Fig. 3a). The model proposed here can handle various types of spatially distributed meteorological data, obtained not only from ground-based gauges but also from radar or satellite observations. In this study, we assumed that evapotranspiration could be ignored during heavy rainfall events and directly used total rainfall for the rainfall–runoff–sediment yield simulation (Tachikawa et al. 2004; Lee et al. 2009).

In order to consider the spatial variability of rainfall, we generated spatially distributed rainfall fields for three flood events due to typhoons (Table 1). The rainfall time series was obtained from four rain gauges and distributed using the Thiessen polygon method. Furthermore, we used hourly temporal resolution of the hydrological data, because the purpose of catchment modeling is to estimate the hydrograph and sedigraph through event-based applications.

The observed discharge and sediment information at the Cheoncheon outlet was required for model calibration and validation; thus, we referred to K-water company annual reports in 2002, 2003, and 2007 for the basic hydrological data associated with water quantity and quality. Regression equations for the rating curves and discharge-sediment curves corresponding to the target events of Table 1 are shown in Table 2. Both discharge and sediment load regression equations for each event are applicable to the overall range of observations from low water level to high water level, which means that the equations may not contain accurate information about extremely high or low water levels during event periods, because those data were acquired from the extrapolated trend lines based on insufficient measurement of samples. Obviously, the reliability of the sediment data is questionable, but this was the best

Table 1 Historical flood events for rainfall–runoff–sediment yield simulation

Event no.	Rainfall duration	Total rainfall (mm)	Typhoon	Use
1	2002.08.30.17:00 to 09.02.19:00	194.82	Rusa	Calibration
2	2003.09.11.21:00 to 09.15.16:00	133.89	Maemi	Validation
3	2007.09.14.06:00 to 09.21.15:00	205.46	Nari	Validation

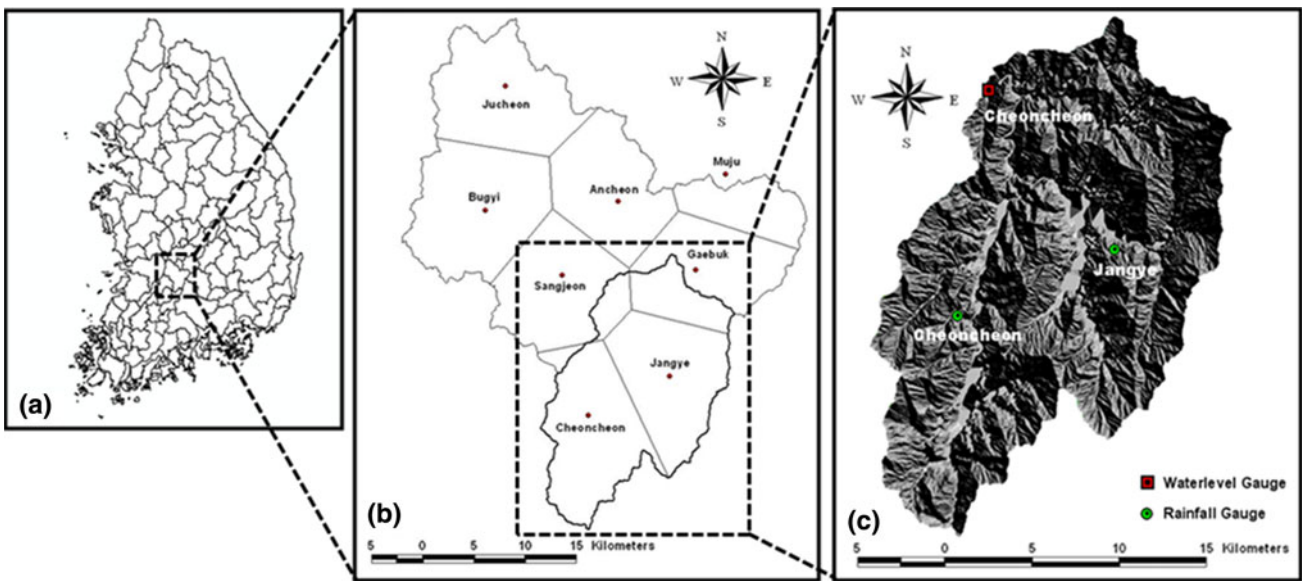

Fig. 3 **a** Map of South Korea, **b** Thiessen polygon of the Yongdam dam basin and **c** hill-shade topography of the study site (Cheoncheon catchment marked by a *bold solid line* in **b**)

Table 2 Regression equations for the observed discharge and sedimentation for the three flood events (K-water 2002, 2003, 2007)

Event no.	Rating curve equation	Discharge-sedimentation loads equation
1	$Q = 24.945 \times (H - 2.281)^{2.448}$	$Q_{sed} = 0.90E - 5 \times Q^{1.700}$
2	$Q = 53.522 \times (H - 2.346)^{2.219}$	$Q_{sed} = 0.50E - 6 \times Q^{1.932}$
3	$Q = 50.403 \times (H - 2.367)^{2.257}$	$Q_{sed} = 0.28E - 5 \times Q^{1.818}$

that could be done, since the Cheoncheon station is the specific experimental site, operated by the K-water company to monitor water quality flowing into the Yongdam dam reservoir.

Model setup and calibration

In this study, the drainage network was represented by a 250 m × 250 m spatial resolution of DEM. Although various DEM spatial resolutions are available in this system, we selected the 250-m DEM because of its computational efficiency (i.e., model run-time) for calibration and application (Lee et al. 2009). Figure 4 shows the Cheoncheon drainage network, which consists of channel and hillslope components.

Land cover information significantly affects the determination of Manning's roughness coefficient, a key parameter to simulate surface flow and resulting soil detachment. We used the values provided by the water management information system (WAMIS; http://www.wamis.go.kr), based on Vieux's proposal (2004), as summarized in Table 3. However, in spite of the soil map with 1:25,000 scales available, parameterization associated with soil hydraulics of both modules remains uncertain due to impossibility of direct use of the soil map properties (i.e., discordance between soil map properties and model parameters used here). Therefore, we assumed that process parameters and some physical parameters in Table 4 are spatially homogenous over the study catchment and then tuned the parameters based on the Rusa event, using the multi-objective shuffled complex evolution metropolis–University of Arizona algorithm (MOSCEM-UA) (Vrugt et al. 2003).

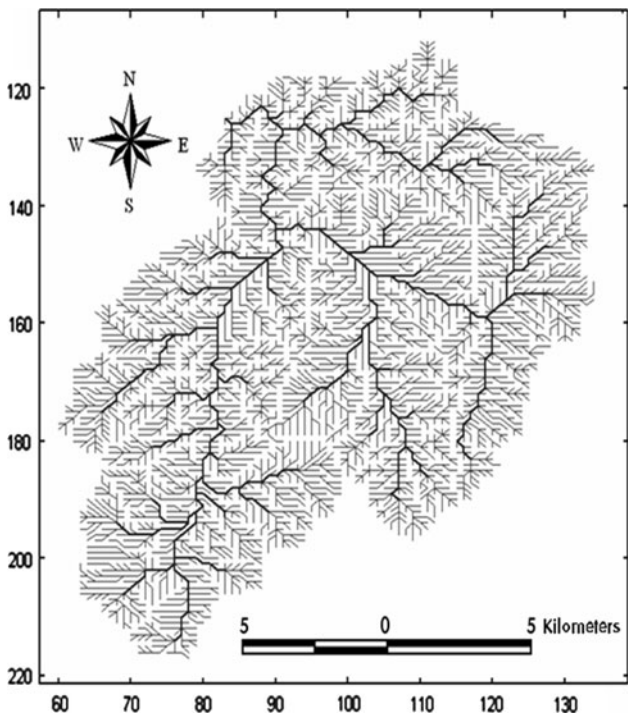

Fig. 4 Drainage network of the Cheoncheon catchment represented by sets of channel (*black line*) and slope (*gray line*) elements

The model used here provides two hydrologic output variables—discharge and sediment discharge at the outlet of interest—such that our target is to find the near-optimal parameter values (i.e., compromise solution among various Pareto optima) leading to a balanced simulation result of both outputs. We selected two objective functions: root mean square error (RMSE) of streamflow and sediment discharge, defined as follows:

$$\mathrm{RMSE}_{str} = \sqrt{\frac{1}{N}\sum_{t=1}^{N}\left(Q_t^{obs} - Q_t(\theta)\right)^2} \quad (8)$$

$$\mathrm{RMSE}_{sed} = \sqrt{\frac{1}{N}\sum_{t=1}^{N}\left(S_t^{obs} - S_t(\theta)\right)^2} \quad (9)$$

where Q_t^{obs} and S_t^{obs} are the observed streamflow and sediment load at time t, respectively, $Q_t(\theta)$ and $S_t(\theta)$ are the simulated streamflow and sediment load at time t, respectively, using the compromise solution parameter set θ, and

Table 3 Roughness coefficient for certain types of land use (Vieux 2004)

No	Land use/land cover classification	Manning's n
1	Water area	0.030
2	Urbanization	0.015
3	Eroded land	0.035
4	Marsh	0.050
5	Grassland	0.130
6	Forest	0.100
7	Paddy field	0.050
8	Cropland	0.035

Table 4 Feasible parameter range for model calibration and compromise parameter values

Parameter	Description	Range of value[a]	Optimal values
d_c	Depth of the unsaturated soil layer (mm)	20–300	31.88
d_s	Depth of the saturated soil layer (mm)	1–700	60.03
k_a	Hydraulic conductivity of the saturated soil layer (m/s)	0.001–0.1	0.007
β	Non-linear exponent constant for the unsaturated soil layer	2–10	7.00
D_{50}	Median grain size (mm)	1–10	9.5
k	Soil detachability (kg/J)	0.0008–0.006	0.002
α	Detachment or deposition efficiency	0.335–1.0	0.86
KE	Total kinetic energy of the net rainfall (J/m^2)	1–30	2.29
$v_{cr}i$	Critical unit stream power (m/s)	0.002–0.100	0.028

[a] Feasible parameter ranges were set up based on reference values by APIP (2008)

N is the number of data available. All MOSCEM-UA algorithmic parameters were determined from the recommended values addressed by Vrugt et al. (2003).

Figure 5 plots the results of the Pareto optimal solutions for the Rusa event, used for model calibration. This figure includes two-dimensional (2D) projections of two criteria solution spaces, which are represented by five hundred Pareto solutions selected from parameter samples after 10,000 iterations of MOSCEM-UA. Here, the gray open circles indicate the Pareto solutions, selected in calibration trials, and the minimum values for each objective function are shown for $RMSE_{str}$ (triangle) and $RMSE_{sed}$ (square); note that criterion $RMSE_{str}$ is minimized at the triangle mark (35.2 (m^3/s)) while criterion $RMSE_{sed}$ is minimized at the square mark [180.2 (mg/L)]. Therefore, the calibration result of MOSCEM-UA is a discrete set of possible parameter sets that represent trade-offs between different optimal ways of constraining the model to be consistent with the observed data.

In this study, we selected the parameter set corresponding to the compromise solution, marked by the diamond in Fig. 5 to obtain equally acceptable simulation results for both hydrologic outputs. The calibrated parameter values of the model are reported in the last column of Table 4; the optimal values fit within the feasible parameter space.

Figure 6 shows the observed versus simulated runoff and sediment discharge for the Rusa flood event. We also used two popular indices to evaluate model applicability: relative error (RE) of peak discharge or peak sediment, and the Nash–Sutcliffe coefficient (NSC), expressed as follows:

$$\mathrm{RE} = \frac{y_t^{\mathrm{peak}} - y_t^{\mathrm{peak}}(\theta)}{y_t^{\mathrm{peak}}} \times 100 \tag{9}$$

$$\mathrm{NSC} = 1 - \frac{\sum_{t=1}^{N} \left(y_t^{\mathrm{obs}} - y_t(\theta)\right)^2}{\sum_{t=1}^{N} \left(y_t^{\mathrm{obs}} - y^{\mathrm{mean}}\right)^2} \tag{10}$$

where y_t^{peak} is the observed peak discharge or peak sediment load at time t, $y_t^{\mathrm{peak}}(\theta)$ is the simulated peak streamflow or peak sediment load at time t using the optimal parameter set θ, and y^{mean} is the average value of the observed variable.

As shown in Table 5 and Fig. 6, the calibrated model provided a well-matched hydrograph temporal pattern over the Rusa flood event (RE: −5.56 %, NSC: 0.85), while the simulated sediment load was overestimated within the range of 1,000–3,500 (mg/L), but was underestimated near peak concentration compared with actual observation (RE: 1.93 %, NSC: 0.90); the deviations in peak discharge and sediment load were 77.03 (m^3/s) and 85.16 (mg/L).

Model application results

We applied the calibrated model for rainfall–runoff–sediment yield simulations for the two historical events: Maemi

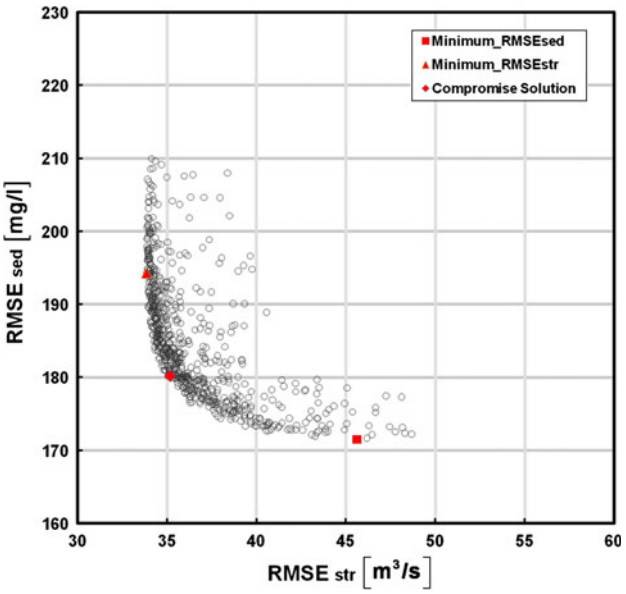

Fig. 5 Pareto solutions and compromise solution of the model after ten thousand iterations using the MOSCEM-UA

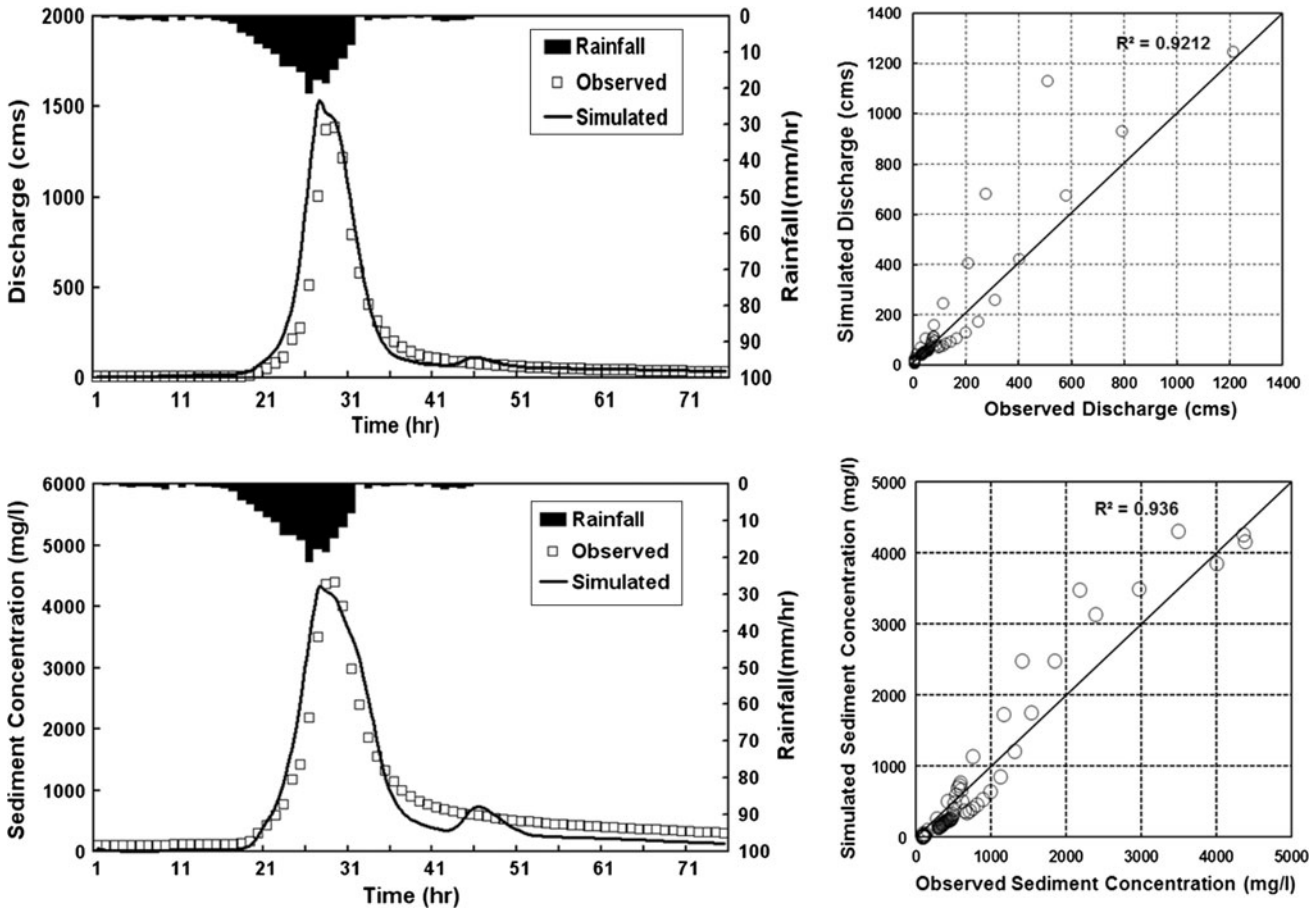

Fig. 6 Comparison of hydrograph and sedigraph data during the Rusa flood event

Table 5 Computed model performance measures for the three events

Typhoon	Criteria	Peak discharge (m^2/s)	Peak sediment concentration (mg/l)
Rusa	Observed	1,384.66	4,391.32
	Simulated	1,461.69	4,306.16
	RE	−5.56 %	1.93 %
	NSC	0.853	0.895
Maemi	Observed	931.90	6,038.06
	Simulated	1,120.91	3,701.51
	RE	−20.28 %	38.70 %
	NSC	0.801	0.711
Nari	Observed	1,134.14	7,160.30
	Simulated	1,119.17	4,135.89
	RE	1.32 %	42.24 %
	NSC	0.692	0.459

and Nari. Figures 7 and 8 show the observed versus simulated runoff and sediment discharge for the Maemi, and Nari flood events, respectively.

For the Maemi and Nari events, the simulated temporal sequences of sedimentation were predicted worse than the runoff in terms of peak flow and time to peak; the simulated sediment loads with high concentration were underestimated compared with the observations of the other validation events, and all model performance measures of sediment discharge were calculated worse than hydrograph simulations, as summarized in Table 5. Despite the marginal differences between the computed and actual hydrographs, the model underestimated sediment discharge from larger than approximately 1,000 (mg/L) for the Maemi and Nari events (see the right panels of Figs. 7, 8).

In general, this kind of prediction uncertainty or error comes from various sources associated with data, model structure, parameters, and so forth in hydrologic modeling. A dominant factor, which leads to a large discrepancy in the sediment load result in this study, may be an insufficient data sampling of sediment loads to produce the runoff–sediment load equations of Table 2. The estimated regression equations (without consideration of very low and high sediment concentration information) are likely to result in a larger difference in sediment load in spite of the marginal change in discharge.

However, it can be said that the sediment yield comparison results during the three events were acceptable,

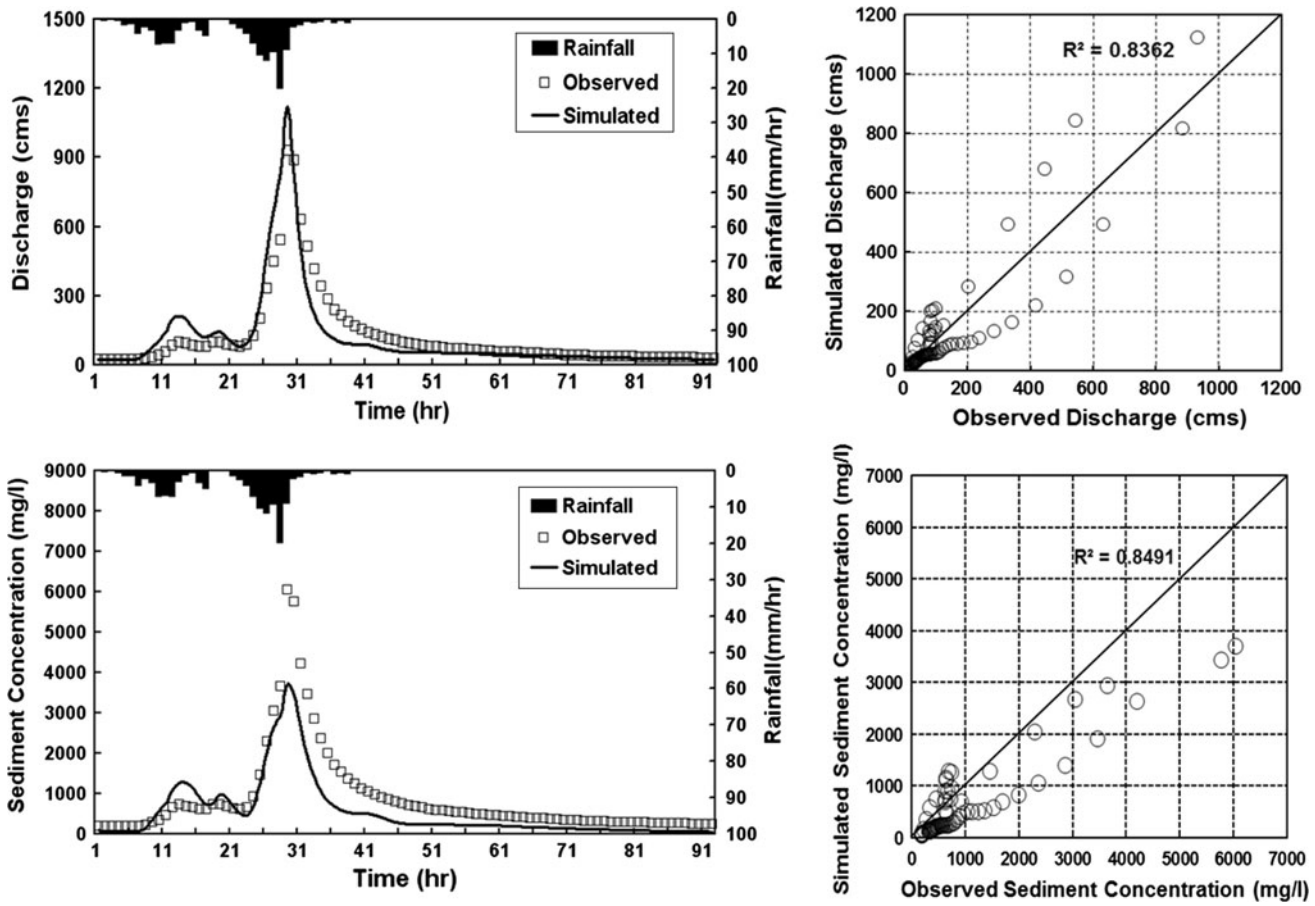

Fig. 7 Comparison of hydrograph and sedigraph data during the Maemi flood event

because the relative errors of the simulated total sediment yields for the three events were within a range of –50 to 200 % of the actual upland erosion from the catchment (5.4, 37.1, and 60.2 % in Rusa, Maemi, and Nari, respectively). This range (−50 to 200 %) is generally considered by sedimentation engineers to be acceptable (Johnson et al. 2000). From these results, the proposed model was able to predict upland erosion from the study catchment.

The distributed rainfall–runoff–sediment yield model used in this study allows modelers to visualize the spatial pattern of erosion at a specific time step, such as the time to peak discharge. Figure 9 shows the spatial dynamic of erosion simulated for the four specific time steps from 10 to 40 h during the Rusa event. Dark colors represent moderate erosion, whereas bright colors represent severe erosion. Increasing rainfall intensity and surface flow from the beginning to the peak of the event clearly shows an increasing erosion rate. In contrast, erosion decreases drastically after rainfall stops (compare figures at the 30 and 40 h time steps). The proposed model represents upland erosion at a catchment scale during a flood event, and the resulting spatial information can be used to distinguish potentially erodible regions and clarify major factors affecting erosion.

Based on acceptable comparisons of model predicted and observed catchment outputs (e.g., runoff and sediment yields), we visualized the net-erosion spatial patterns, produced by soil redistribution due to dynamic processes of erosion and deposition during each event. The results are illustrated in Fig. 10. The plus and minus marks represent erosion and deposition, respectively. Maximum erosion was obtained at 0.6 cm (Rusa), 0.39 cm (Maemi), and 1.58 cm (Nari), whereas maximum deposition was simulated at 4.76 cm (Rusa), 2.42 cm (Maemi), and 3.1 cm (Nari). In general, convex ridge tops and mid-slope knobs had the most erosion, while concave regions along river channels receiving convergent runoff exhibited sediment deposition. Moreover, many mid-slope cells showed either erosion or deposition, suggesting that they were soil transport zones. This concurred with Busacca et al. (1993).

Because the energy imparted to the soil from rainfall is dependent on drop size, fall velocity, and rainfall intensity, the net-erosion values were spatially distinguished according to the four Thiessen polygons used in this study

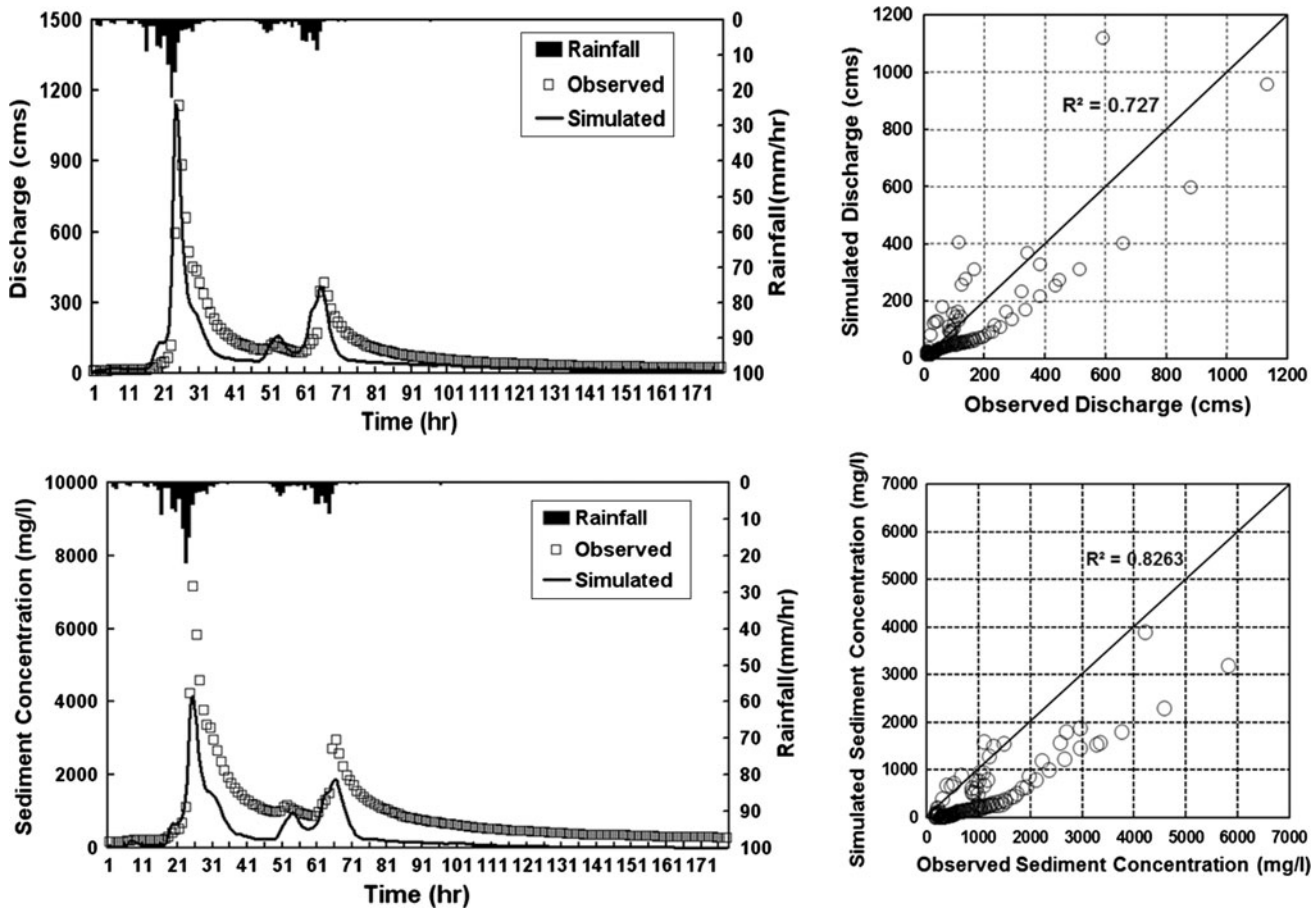

Fig. 8 Comparison of hydrograph and sedigraph data during the Nari flood event

(see Fig. 3a). Although the Maemi event simulation result showed an indistinguishable net-erosion spatial pattern (due to relatively spatially uniform rainfall intensity among the four gauging stations not found in the other two events), Fig. 10 clearly shows how spatially different rainfall fields, generated by the Thiessen method, influenced catchment erosion and deposition processes.

Analysis of factors influencing soil erosion and deposition

As previously stated, environmental conditions determine erosion and deposition rates. The four environmental factors that determine water erosion and sedimentation are climate, soil, topography, and land use. Each factor operates both independently and interactively. In this study, we focused on the effects of topographic and climatic factors on net-erosion.

For analysis of the relationship between topographic factors and net-erosion, we calculated the hillslope flow path distance (Turker et al. 2001) and local slope (Ijjasz-Vasquez and Bras 1995) at each grid cell over the catchment and then compared them with the net-erosion values of Fig. 10. Note that the hillslope flow path distance is defined by following the steepest descent path downslope until a channeled pixel is first reached, and the local slope is calculated by dividing the difference in elevation between neighboring grids in the steepest downstream direction by the length between grid centers. The calculated hillslope flow path distance and local slope of the study catchment are illustrated in Fig. 11.

As shown in Fig. 11, the grid cells near channel networks had a shorter hillslope flow path distance and milder slope steepness than the grid cells far from the channel networks, particularly located in the catchment boundary. The plot of Fig. 12a for hillslope flow path distance versus local slope clearly supports the spatial relation of both topographic factors in Fig. 11; the local slope became steeper as the hillslope flow path distance increased. In Fig. 12b, erosion was evenly distributed over the entire range of hillslope flow path distance regardless of flood events, whereas deposition occurred irregularly. An interesting finding was that deposition nearly disappeared on

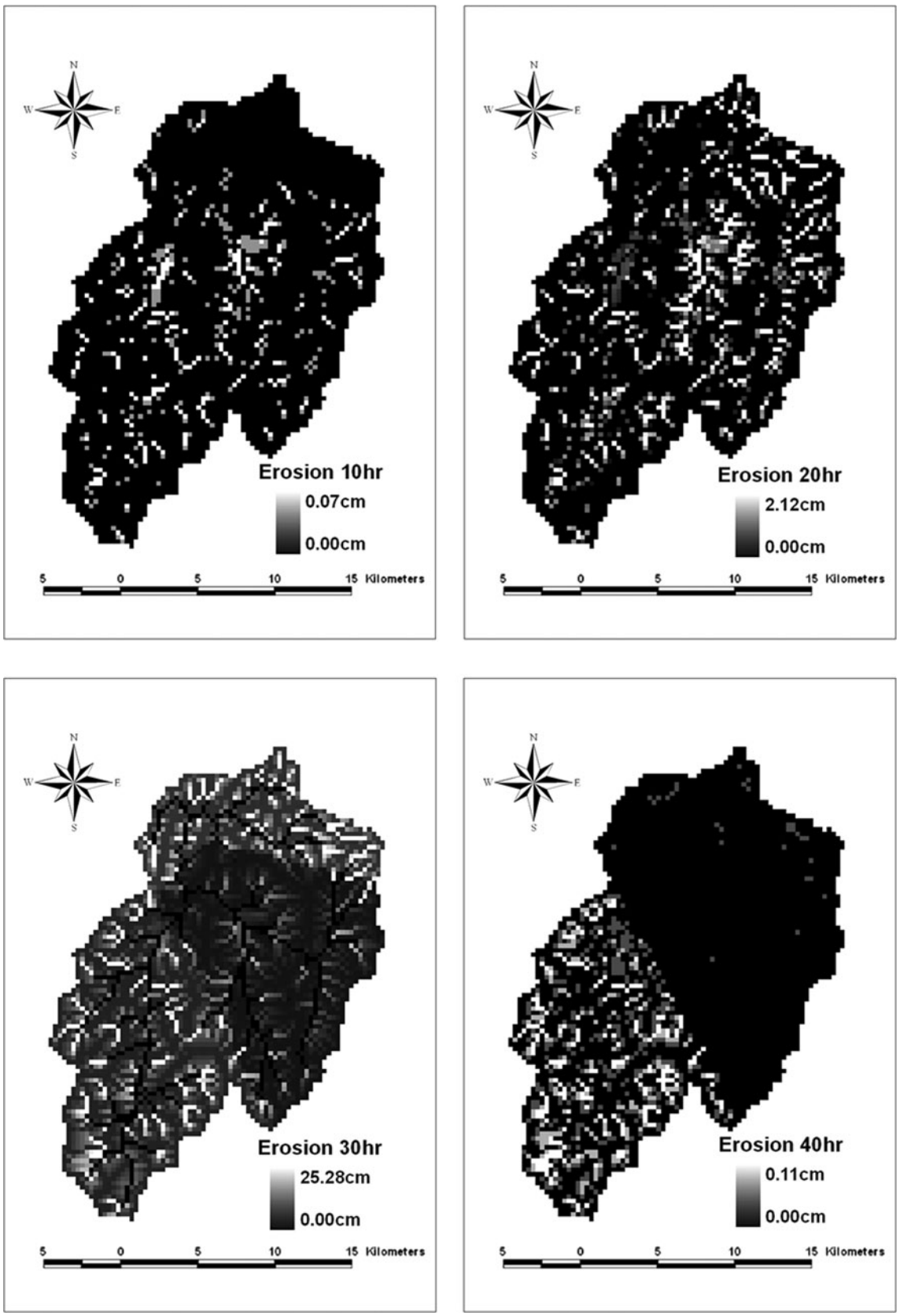

Fig. 9 Time series of spatially distributed erosion rate (cm) within the study site during the Rusa event

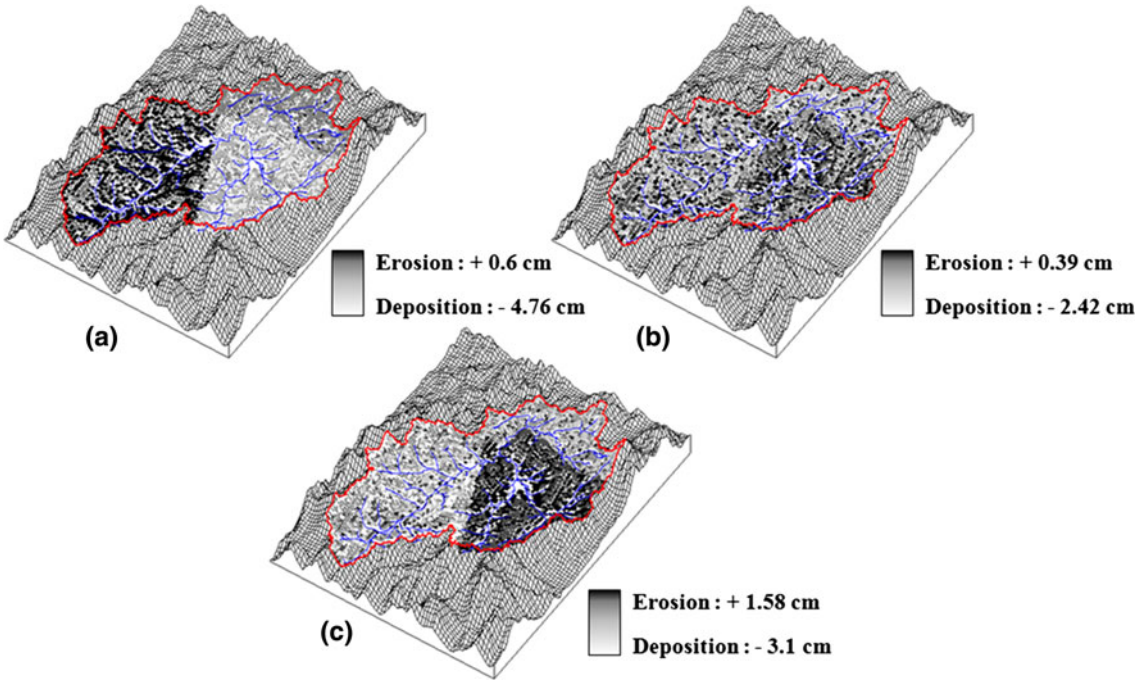

Fig. 10 Soil erosion and deposition in the Cheoncheon catchment for the three events: **a** Rusa (2002); **b** Maemi (2003); **c** Nari (2007)

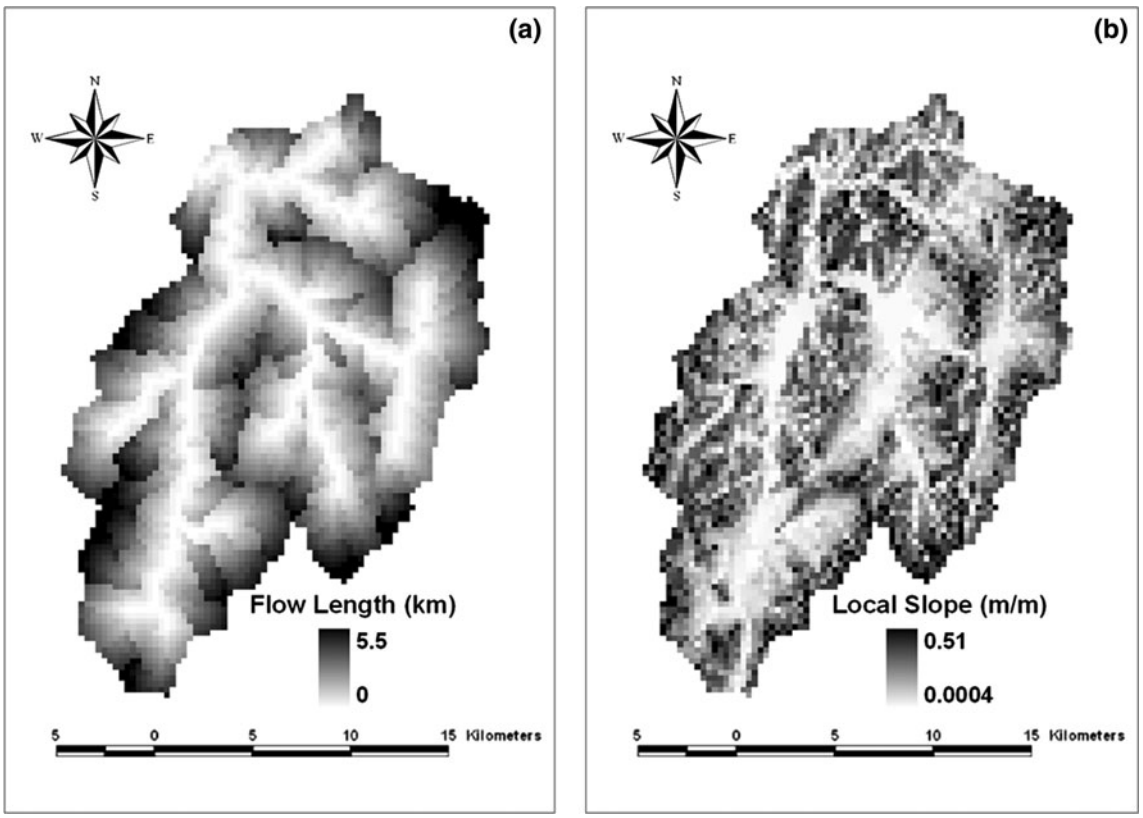

Fig. 11 Maps of **a** hillslope flow path distance and **b** local slope of the Cheoncheon catchment

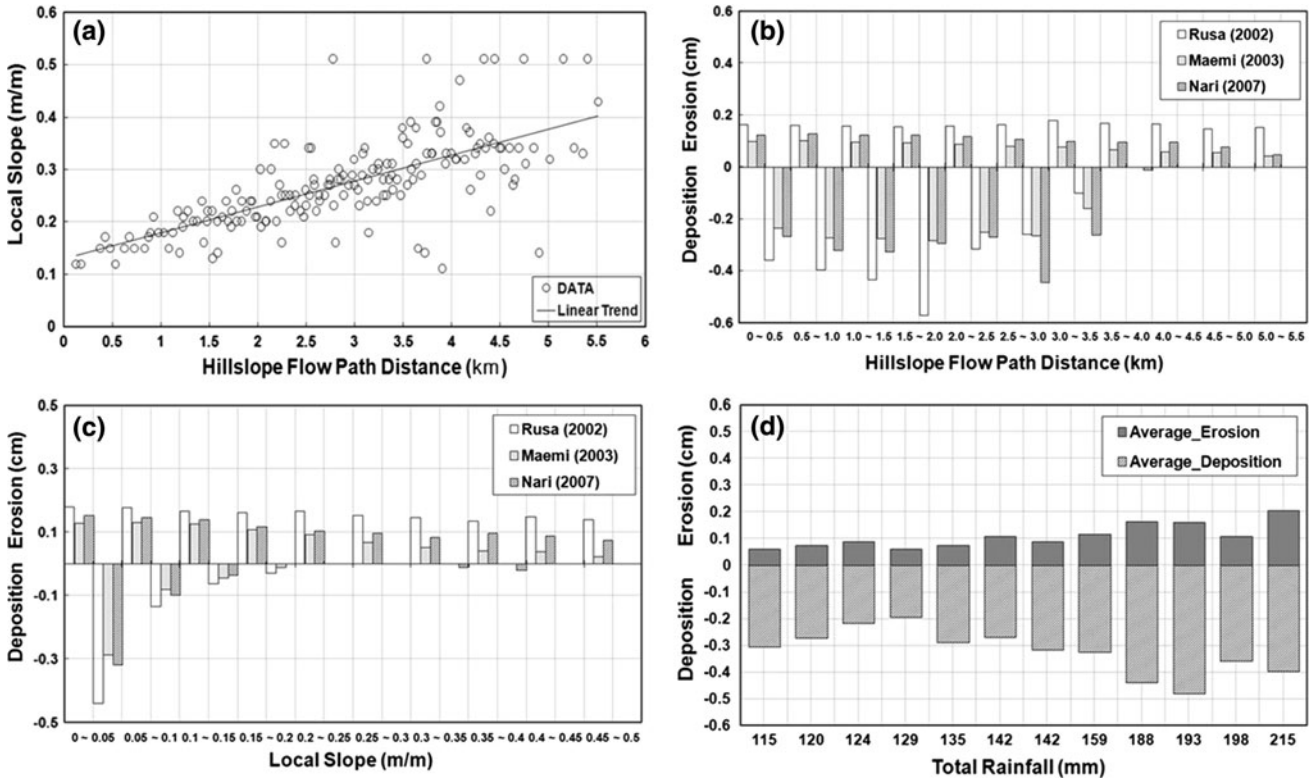

Fig. 12 *Plots* of **a** hillslope flow path distance versus local slope; **b** hillslope flow path distance versus erosion and deposition; c local slope versus erosion and deposition; **d** total rainfall versus erosion and deposition

upland cells where the hillslope flow path distance was longer than 3.5 (km); erosion, rather than deposition, predominated in these cells.

Furthermore, in Fig. 11c, deposition decreased drastically as the local slope became steeper, whereas erosion changed slightly; in particular, deposition did not occur on the cells with the local slope steeper than 0.2 (m/m). These results suggest that the downstream areas near channel networks are significantly affected by deposition rather than erosion, which coincides exactly with the spatial distribution of erosion and deposition in Fig. 10. However, it is not yet possible to determine the erosion-dominant factor from the two topographic factors used in this study, as erosion does not show obvious upward or downward trends with respect to these topographic factors.

We additionally assessed the effect of rainfall, as an indicator of climate, on erosion. For this experiment, we calculated accumulated rainfall on each grid cell over the catchment during the three flood events and then sorted the average values of erosion or deposition corresponding to grid cells with identical total rainfall in ascending order of the total rainfall, as shown in Fig. 12d. Note that many grid cells had only four values of accumulated rainfall. This was due to the number of Thiessen polygons based on four ground rain gauges for each flood event. Therefore, we extracted the cells corresponding to individual rainfall amount of 12 total values (calculated by multiplying three flood events and four gauge stations) to obtain the average erosion and deposition rates. Figure 12d shows the gradual upward trend of erosion, whereas deposition fluctuated across the range of accumulated rainfall. Although sufficient spatial data of rainfall were unavailable to plot the relationship between total rainfall and erosion or deposition, it is clear from Fig. 12 that soil erosion was closely related to rainfall rather than to topographic factors. If radar or satellite radar data are applicable to the model, more details regarding the effect of rainfall on soil erosion modeling will be discussed.

Concluding remarks

Quantitative information on soil erosion and deposition rates in time and space is often not available for a variety of soil erosion problems, so it has been difficult to prepare countermeasures against such problems. Thus, surface runoff and soil erosion simulation models are useful, because they can provide basic and important information such as runoff, sediment yield, and spatial distribution of erosion and deposition rates to be used in assessing alternative strategies for soil and water conservation, not only in monitored sites but also in ungauged catchments. This

study applied a process-oriented distributed hydrologic model for the simultaneous simulation of rainfall–runoff and erosion-sedimentation yield in the small mountainous catchment of Korea and investigated the effects of topographic (hillslope flow path distance and local slope) and climatic (accumulated rainfall) factors on erosion and deposition at a catchment scale.

The major findings of this study were as follows:

1. The proposed model properly simulated the hydrological responses (such as runoff and sediment load) of the study catchment, subject to spatially and temporally variable rainfall fields, generated by the Thiessen method. At the Cheoncheon outlet, which has hydrological measurement equipment, simulated peak discharge and time to peak discharge values were close to the observed values, although the simulated high concentration sediment loads were underestimated compared with actual observations. Total sediment yield during the flood events was within the acceptable range (−50 to 200 %). Thus, the proposed model is a useful tool to predict hydrological and soil erosion processes during flood rainfall events on a catchment scale.
2. Spatial information with respect to erosion and deposition at simulation time steps of interest can be visualized on a grid cell with colored values using GIS tools. Deposition was observed in the grid cells along the channel network, and erosion occurred over a wide area (more so in the upstream region with steep slopes than in the downstream region with gentle slopes). For more detailed analysis of the effects of topographic factors on erosion and deposition, we plotted the local slope variation against hillslope flow path distance. The local slope increased gradually as the hillslope flow path distance from the channel network became greater. Deposition was strongly affected by the catchment topography; the critical values of both topographic factors, providing only deposition, were observed at 3.5 (km) (hillslope flow path distance) and 0.2 (m/m) (local slope), respectively, whereas erosion took place uniformly over the entire ranges of the topographic factors.
3. The eroded sediment was very sensitive to the applied spatial pattern of rainfall amount generated by the Thiessen method with the four rain gauge stations. Erosion increased gradually as rainfall amounts increased, but deposition responded irregularly to variations in total rainfall. Independent assessments of the effects of topography and rainfall suggested that deposition was relatively sensitive to topography, whereas rainfall was a primary factor affecting erosion.

The physically based hydrological model used in this study did not always produce perfect results for a number of flood events; this is due to various prediction uncertainty sources involved in modeling. To reduce data uncertainty and improve simulation accuracy in rainfall–runoff–sediment yield modeling, continuous monitoring of sediment is essential. Moreover, the model needs to make full use of GIS-based information regarding model parameters to reduce parameter uncertainty by minimizing calibration trials.

Localization of erosion-prone areas and quantitative estimation of soil loss rates with reliable accuracy is of extreme importance for designing and implementing appropriate erosion control or soil and water conservation practices. If various types of spatial information regarding rainfall, topography, land cover/use, and geology are sufficiently available, this distributed rainfall–runoff sediment yield model can be used as a fundamental tool not only to provide spatial information of erosion- and deposition-prone areas but also to evaluate the effects of land use changes, such as deforestation and urbanization in the future.

Acknowledgments This study was supported by the National Research Foundation of Korea Grant funded by the Korean Government (NRF-2010-355-D00062) and the Construction Technology Innovation Program (08-Tech-Inovation-F01) through the Research Center of Flood Defense Technology for Next Generation in Korea Institute of Construction & Transportation Technology Evaluation and Planning (KICTEP) of the Ministry of Land, Transport and Maritime Affairs (MLTM).

References

APIP (2008) Watershed hydrological modeling based on runoff and sediment transport processes: a physically-based distributed model and its lumping. Master's Thesis, Kyoto University

Busacca AJ, Cook CA, Mulla DJ (1993) Comparing landscape scale estimation of soil erosion in the Palouse using Cs-137 and RUSLE. J Soil Water Conserv 48:361–367

Chae J, Jung M, Torii N, Okimura T (2010) A risk evaluation method of slope failure due to rainfall using a digital terrain model. J Korea Soc Civil Eng 30(6C):219–229 (in Korean)

De Roo APJ, Wesseling CG, Ritsems CJ (1996a) LISEM: a single-event physically based hydrological and soil erosion model for drainage basins. I: theory, input and output. Hydrol Process 10:1107–1117

De Roo APJ, Offermans RJE, Cremers NHDT (1996b) LISEM: a single-event physically based hydrological and soil erosion model for drainage basins. II: sensitivity analysis, validation and application. Hydrol Process 10:1119–1126

Flanagan DC, Nearing MA (1995) USDA-water erosion prediction project hillslope profile and watershed model documentation. NSERL Report No. 10, USDAARS National Soil Erosion Research Laboratory, West Lafayette, Indiana

Foster GR (1982) Modeling the soil erosion process. In: Haan CT, Johnson HP, Brakensiek DL (eds) Hydrologic modeling of small watersheds. ASAE Monograph No. 5, ASAE, St. Joseph, pp 297–380

Foster GR, Meyer LD (1977) Soil erosion and sedimentation by water: an overview. In: ASAE (ed) Proceedings of the national symposium on soil erosion and sedimentation by water, pp 1–13

Govers G (1990) Empirical relationships on the transporting capacity of overland flow. IAHS Publ 189:45–63

Ijjasz-Vasquez EJ, Bras RL (1995) Scaling regimes of local slope versus contributing area in digital elevation models. Geomorphology 12:299–311

Jetten V, Govers G, Hesse R (2003) Erosion models: quality and spatial predictions. Hydrol Process 17:887–990

Johnson BE, Julien PY, Molnar DK, Watson CC (2000) The two dimensional-upland erosion model CASC2D-SED. J AWRA 36(1):31–42

Julien PY, Saghafian B, Ogden FL, American Water Resources Association-AWRA (1995) Raster-based hydrologic modeling of spatially-varied surface runoff. Water Resour Bull 31(3):523–536

Kalin L, Hantush MM (2003) Evaluation of sediment transport models and comparative application of two watershed models. National Risk Management Research Laboratory, Office of Research and Development, U.S. Environmental Protection Agency

K-water (2002) Hydrological investigation report of Yongdam dam basin

K-water (2003) Hydrological investigation report of Yongdam dam basin

K-water (2007) Hydrological investigation report of Yongdam dam basin

Lane LJ, Shirley ED, Singh VP (1988) Modelling erosion on hillslopes. In: Anderson MG (ed) Modelling geomorphological systems, chap 10. Wiley, Chichester

Lee J, Jung J, Lee S (2007) A study on characteristic analysis of soil erosion models in Korea and foreign country. National Institute for Disaster Prevention, Nagaoka (in Korean)

Lee J, Jung J, Huh B, Lee S (2008) A study on improvement of applicability of soil erosion prediction models in practical use. National Institute for Disaster Prevention, Nagaoka (in Korean)

Lee G, Tachikawa Y, Takara K (2009) Interaction between topographic and process parameters due to the spatial resolution of DEMs in distributed rainfall-runoff modeling. J Hydrol Eng 14(10):1059–1069

McCool DK, Brown LC, Foster GR, Mutchler CK, Meyer LD (1987) Revised slope steepness factor for the universal soil loss equation. Trans ASAE 30(4):1387–1396

McCool DK, Foster GR, Mutchler CK, Meyer LD (1989) Revised slope length factor for the universal soil loss equation. Trans ASAE 32(5):1571–1576

Morgan RPC, Quinton JN, Rickson RJ (1992) EUROSEM documentation manual. Silsoe College, Silsoe

Morgan RPC, Quinton JN, Smith RE, Govers G, Poesen JWA, Chisci G, Torri D (1998) The European soil erosion model (EUROSEM): a dynamic approach for predicting sediment transport from fields and small catchments. Earth Sur Process Landf 23:527–544

Morris GL, Fan J (1997) Reservoir sedimentation handbook. McGraw-Hill, New York

Nearing MA, Page DI, Simanton JR, Lane LJ (1989) Determining erodibility parameters from rangeland field data for a process-based erosion model. Trans ASAE 32(3):919–924

O'Callaghan JF, Mark DM (1984) The extraction of drainage networks from digital elevation data: computer vision. Graph Image Process 120:328–344

Park M, Son K (1998) Study on the sediment yield estimation due to land development (I), Research Report No. 97-04. National Institute for Disaster Prevention, Nagaoka (in Korean)

Sayama T (2003) Evaluation of reliability and complexity of rainfall-sediment-runoff models. Master's Thesis, Kyoto University

Shiiba M, Ichikawa Y, Sakakibara T, Tachikawa Y (1999) A new numerical representation form of basin topography. J Hydraul Coast Environ Eng, JSCE 621:1–9 (in Japanese)

Singh VP (2001) Kinematic wave modeling in water resources: a historical perspective. Hydrol Process 15:671–706

Storm DE, Barfield BJ, Ormsbee LE (1990) Hydrology and sedimentology of dynamic rill networks. I. Erosion model for dynamic rill networks, Research Report No. 178, Kentucky Water Resources Research Institute, University of Kentucky, Lexington, KY

Tachikawa Y, Nagatani G, Takara K (2004) Development of stage-discharge relationship equation incorporating saturated–unsaturated flow mechanism. Ann J Hydraul Eng, JSCE 48:7–12 (in Japanese)

Takasao T, Shiiba M (1988) Incorporation of the effect of concentration of flow into the kinematic wave equations and its applications to runoff system lumping. J Hydrol 102:301–322

Toy TJ, Foster GR, Renard KG (2002) Soil erosion: processes, prediction, measurement and control. Wiley, New York

Turker GE, Catani F, Rinaldo A, Bras RL (2001) Statistical analysis of drainage density from digital terrain data. Geomorphology 36:187–202

Vente JD, Poesen J (2005) Predicting soil erosion and sediment yield at the basin scale: scale issues and semi-quantitative models. Earth Sci Rev 71:95–125

Vieux BE (2004) Distributed hydrological modeling using GIS. Kluwer, Dordrecht

Vrugt JA, Gupta HV, Bouten W, Sorooshian S (2003) A shuffled complex evolution metropolis algorithm for optimization and uncertainty assessment of hydrologic model parameters. Water Resour Res 39(8):1201. doi:10.1029/2002WR001642

Woolhiser DA, Smith RE, Goodrich DE (1990) KINEROS, a kinematic runoff and erosion model: documentation and user manual, USDA, ARS-77

Yang CT (1972) Unit stream power and sediment transport. J Hydraul Div ASCE 98(HYI0):1805–1826

Yang CT (1973) Incipient motion and sediment transport. J Hydraul Div ASCE 99(HY10):1679–1704